Asymmetry-induced transient gel formation in fluid lipid membranes

Emad Pirhadi, Xin Yong*

Department of Mechanical and Aerospace Engineering, University at Buffalo, Buffalo, New York 14260

*E-mail: xinyong@buffalo.edu

Abstract

Compositional asymmetry is a defining feature of cellular membranes, controlling permeability, protein activity, cholesterol dynamics, and shape remodeling. This asymmetry can create a stress imbalance, with the two leaflets experiencing opposing tensions, though direct experimental measurement of leaflet stress remains challenging. Such a stress imbalance can compress one leaflet and trigger a fluid-to-gel phase transition, which reduces membrane fluidity and markedly increases bending rigidity. These phenomena raise a key question of how membranes respond mechanically before crossing the transition threshold, a regime that remains relevant to biological functions. Here, we combine extensive all-atom and coarse-grained molecular dynamics simulations to examine how stress asymmetry modulates membrane structure and mechanics near the transition point. Using POPE and DLPC bilayers as model systems, we find that moderate asymmetry induces transient gel-like domains that continuously form and dissolve, amplifying undulations and lowering bilayer rigidity. Beyond the gelation threshold, the trend reverses and the bilayer stiffens, resulting in a non-monotonic dependence of rigidity on asymmetry. Moreover, our results reveal distinct curvature preferences of fluid and gel phases. Extending this analysis to a multicomponent bacterial outer membrane, we demonstrate that stress asymmetry can trigger transient gel-like domain formation even in complex lipid mixtures. This provides a proof of principle that differential stress modulates membrane mechanics by inducing either softening or stiffening, complementing the effects of molecular composition. Our findings elucidate how cells might exploit the stress-curvature-phase coupling to tune membrane rigidity under near-physiological conditions.

Significance statement

Cell membranes are selectively permeable bilayers composed of different lipids that are unevenly distributed both across the two leaflets and within each leaflet. These structural features influence how membranes maintain their integrity, position proteins, and send signals. While each feature has been studied separately, the direct influence of leaflet asymmetry on lateral lipid organization remains unclear. Using molecular simulations, we show that leaflet asymmetry can drive lipids to cluster into coexisting fluid and gel domains at body temperature. This reorganization softens the membrane and enhances its fluctuations. Our findings reveal a direct link between leaflet asymmetry and lateral

structure, shedding light on how cells can tune membrane properties to regulate communication, transport, and adaptation to stress.

Introduction

Cellular membranes function as dynamic, selective barriers that maintain homeostasis while supporting diverse processes such as signaling, trafficking, and mechanical deformation.(1-3) These essential roles are closely linked to two defining biophysical features: compositional asymmetry between the two leaflets and lateral heterogeneity within each leaflet.(4-7) The asymmetric distribution of lipids is essential for numerous cellular functions, including vesicle formation, membrane trafficking, and signal transduction.(8-11) By creating differential leaflet stress, asymmetry can drive or suppress curvature generation, regulate membrane protein orientation and activity, and modulate the recruitment of curvature-sensing proteins.(12-16) In parallel, lateral heterogeneity organizes membrane components into dynamic functional domains that further influence protein's activity.(17-22) Laterally, lipid bilayers can adopt a phase-separated state, with liquid-ordered (Lo) domains characterized by tightly packed and more ordered lipids coexisting with liquid-disordered (Ld) regions that are more fluid and loosely packed.(23) Lateral phase separation in bilayers is known to depend on lipid headgroup chemistry, tail length and saturation, charge, and the presence of cholesterol.(23-25) Cholesterol, in particular, plays a dual role by stabilizing both ordered and disordered phases depending on the surrounding lipid environment.(26, 27) Moreover, lipid phase behavior is highly sensitive to temperature; below a lipid's main phase transition temperature (T_m), the bilayer can transition from a fluid-to-gel phase, characterized by reduced lateral mobility and increased stiffness.(28-30)

While the thermotropic behavior of membranes has been extensively studied, recent findings suggest that stress asymmetry can also influence phase behavior. Coarse-grained simulations by Hossein and Deserno (31, 32) demonstrated that stress asymmetry can drive phase transitions, even at constant temperature. Depending on proximity to T_m, such stress can induce fluid-gel coexistence and alter bilayer mechanical properties.(33) Importantly, while both Lo and gel (Lβ) phases involve high tail ordering, they differ fundamentally in lateral dynamics: Lo domains are fluid and cholesterol-rich, whereas gel domains are solid-like and typically cholesterol-poor.(34) From a physical standpoint, the gel phase exhibits unique and intriguing properties, however, its biological relevance remains debated as extreme rigidity can compromise membrane function and cell viability.(35-37) In both eukaryotic and prokaryotic cells, lipid compositions are tightly regulated to maintain a T_m slightly above the culture temperature.(38, 39) This raises the intriguing possibility that cells exploit stress asymmetry to tune membrane behavior near the phase transition boundary, maintaining global fluidity while enabling transient formation of ordered domains.

In this study, we employ extensive all-atom and coarse-grained molecular dynamics simulations to investigate how stress asymmetry, introduced via leaflet lipid mismatch, modulates phase behavior and mechanical properties in both simplified and physiologically relevant membrane models. We find that, near the phase transition limit, bilayers remain globally fluid yet form transient gel-like domains that display curvature sensitivity, enhanced undulations, and reduced bending rigidity at a constant physiologically relevant temperature. Furthermore, under large differential stress, our all-atom simulations confirm recent observations of membrane stiffening and gel-phase formation (31-33) in coarse-grained studies. This reveals a two-staged mechanical response of membrane to asymmetry: softening near the transition threshold, followed by gelation-induced stiffening. Together, our results suggest a mechanistic framework by which cells tune their membrane deformability and lateral organization via leaflet asymmetry. This mechanism may enable adaptive responses to environmental cues, regulate protein activity, or enhance resistance to membrane-targeting agents such as antimicrobial peptides. By linking compositional asymmetry to dynamic control over phase behavior, this study provides new insights into how both eukaryotic and prokaryotic cells may regulate membrane mechanics at physiological temperatures.

Results

Leaflet asymmetry drives a fluid-to-gel phase transition. We investigated how leaflet asymmetry influences bilayer lateral heterogeneity using all-atom and coarse-grained molecular dynamics simulations. Asymmetry was introduced by creating a lipid number mismatch between the two leaflets, quantified as

$$\Delta n = 100(n_u - n_l)/(n_u + n_l)$$

where n_u and n_l are the numbers of lipids in the upper and lower leaflets, respectively. Δn represents the percentage difference in lipid count between leaflets and is directly related to differential stress: overpopulating one leaflet imposes negative tension (compression) on that leaflet and positive tension (extension) on the opposite leaflet. Simulations were performed with 1-palmitoyl-2-oleoyl-sn-glycero-3-phosphoethanolamine (POPE) (Fig. 1A,B), chosen for the significant presence of PE in plasma membranes (particularly the cytoplasmic leaflet) and established role in membrane budding and cell division.(40-42) Bilayer phase separation has been shown to be size dependent, thus we modeled three sets of bilayers with approximately 200, 400, and 800 lipids per leaflet (Table S1). Fig. S1 shows that phase separation behavior is consistent among these system sizes. The rest of our analysis on POPE bilayers is done on the ~400 lipid/leaflet set.

As shown in Fig. 1C, increasing Δn leads to a sharp decrease in the average area per lipid (APL) in the upper leaflet at $\Delta n \approx 10.1\%$, consistent with enhanced lipid packing. At this same degree of asymmetry, we observed a marked increase in lipid tail carbon-

carbon order parameters (S_{cc}) and bilayer thickness (z_{pp}) (Fig. 1D,E), signatures of a transition to the gel phase.(43) Beyond this threshold, the gel-phase upper leaflet dominates overall bilayer properties, as reflected in the bilayer thickness. Notably, prior to the transition, the extended (positive tension) lower leaflet exhibits greater sensitivity to asymmetry. This is evident from the more pronounced deviation in APL and S_{cc} of the extended leaflet before the phase transition (Fig. 1C,D). As a result, bilayer thickness decreases by approximately 0.05 nm due to an overall less ordered bilayer within this limit. These changes indicate that differential stress affects bilayer properties even in the absence of a phase transition.

Ordered and disordered domains display opposite curvature preferences in fluid–gel mixture. Above the asymmetry threshold $\Delta n \geq 10.1\%$, the compressed leaflet exhibits a mixture of ordered, gel domains and disordered, fluid regions, consistent with the observations in coarse-grained simulations of 1,2-dilauroyl-sn-glycero-3-phosphocholine (DLPC) bilayers reported by Foley et al.(33) We mapped the instantaneous structural properties of individual lipids in the compressed leaflet and visualized their spatial distribution as heatmaps (see Fig. 2A-C). The distinct degree of lipid packing visible in these figures, together with quantitative differences in tail order parameter, tail height, and area per lipid, confirms the presence of two structurally distinct domains. This coexistence remains stable throughout our analysis simulation time (2 μs), with small fluctuations in the gel domain size (see Videos S1-3).

To examine curvature sensitivity, we computed the instantaneous curvature experienced by each lipid from the Fourier spectrum of bilayer height fluctuations(44, 45):

$$h_{\mathbf{q}} = \sum_{p} h_p e^{-i\mathbf{q}\cdot\mathbf{r}_p}$$

$$c(x,y) = -\nabla^2 h(x,y)$$

$$c(x,y) = -\sum_{q_{min}}^{q_{max}} h_{\mathbf{q}} |\mathbf{q}|^2 \, e^{i\mathbf{q}\cdot\mathbf{r}}$$

where $h_{\mathbf{q}}$ is the Fourier amplitude of mode $\mathbf{q}$, $\mathbf{r}_p$ and h_p are the position and height of grid point p, q_{min} and q_{max} define the range of $\mathbf{q}$ used in calculation, and $c(x,y)$ is the local curvature. We focused on low $\mathbf{q}$ modes ($q_{max} = 0.8\ \mathrm{nm}^{-1}$) to capture large-scale undulations while avoiding significant noise in larger $\mathbf{q}$ modes. Representative snapshots (see Fig. 2D) show that gel domains are consistently registered with regions of positive curvature, whereas fluid regions occupy areas of negative curvature. This curvature partitioning persists throughout the entire 2 μs of our analysis trajectory.

To quantify structural differences between phases, we applied a Hidden Markov Model (HMM),(46) which uses an unsupervised machine learning algorithm to classify each lipid as gel or fluid.(47, 48) We train the model using three per-lipid attributes: tail order parameter, tail height, and area per lipid. Assuming a binary phase state, the HMM labeled each lipid in every frame, enabling phase-specific curvature statistics. As shown in Fig. 3, the curvature difference between gel and fluid domains increases with asymmetry and exhibits a distinct jump at the phase transition threshold ($\Delta n \geq 10.1\%$). These findings reveal that asymmetry-induced phase coexistence is accompanied by distinct curvature preferences of fluid and gel domains.

Transient domain formation drives bilayer softening near the asymmetry-induced phase transition. The gel fraction in the compressed leaflet increases gradually with Δn until the large-scale phase transition ($\Delta n \approx 10.1\%$), where it exhibits a sharp jump (Fig. 4A). Beyond this point, gel domain growth is attenuated, and 100% gel fraction would likely require asymmetry levels that compromise bilayer stability. Herein, we focus on the pre-transition regime $8.6\% \leq \Delta n \leq 10.1\%$, where the bilayer remains globally fluid, which is a physiologically plausible state.

HMM-based phase mapping and spatiotemporal domain analysis reveal that in this range, small gel-like domains form transiently within the fluid leaflet (see Videos S1–S3). A gel-like domain was defined as a minimum of 4 neighboring gel-state lipids persisting for at least 10 frames. The number of domains and their maximum lifetime both increase with asymmetry until the global transition, at which point separate domains merge into a single stable one during the entire span of simulation. In the pre-transition regime, more than 200 domains form during the entire trajectory, with maximal lifetimes of larger than 100 ns. The combination of this clustering behavior and a gel fraction of 20-30% (Fig. 4B,C) indicates highly dynamic phase heterogeneity without complete solidification in the compressed leaflet.

Previous work by Hossein and Deserno (31) reported an asymmetry-induced increase in the bilayer bending modulus following a fluid-to-gel phase transition, consistent with thermodynamic expectations for comparing homogeneous gel and fluid phases. In contrast, our analysis targets the pre-transition regime, where transient domains appear. Here, we find evidence of softening rather than stiffening in that regime.

We quantified mechanical properties by computing the area compressibility modulus (K_A) and bending modulus (κ) as functions of number asymmetry (Δn). The area compressibility modulus was calculated from equilibrium fluctuations in bilayer area under the zero membrane tension condition.(49) The decrease in K_A with increasing asymmetry in the pre-transition regime indicates bilayer softening, which is followed by a sharp increase upon gelation (Fig. 5B). For κ, we applied three standard methods, height fluctuations in the Fourier space (hq),(50, 51) transverse-curvature-bias (TCB),(44) and

real-space fluctuations (RSF).(52, 53) Unfortunately, all three methods rely on assumptions valid only in the fluid phase,(54) and thus fail in the gel state. This can be seen by the power spectra of undulations that illustrate a pronounced q-dependence in the gel state, highlighting the breakdown of continuum elastic theory (see Fig. S2). The RSF method, shows a monotonic increase in κ with increasing asymmetry, even before gelation. However, this apparent stiffening may be an artifact as RSF is largely insensitive to large-scale fluctuations and instead reflects local lipid splay dominated by short-range interactions. As a result, while RSF is a useful tool for homogeneous membranes, it likely reports local lipid ordering rather than true bending elasticity in our heterogeneous systems (see Fig. S3). To the extent of our knowledge, the buckling method (55, 56) used often for coarse-grained models may be the only method capable of calculating the bending modulus in the gel phase. However, even this method hinges on a few critical assumptions, which may not be fully satisfied in the presence of inhomogeneous gel domains.(32) Additionally, because the buckling method imposes curvature, it could inadvertently promote phase transitions in membranes near T_m, especially if curvature favors the gel phase over the fluid phase (see Fig. 3). This may explain the apparent pre-transition stiffening reported by Ref. (31).

The hq method, which is considered the gold standard for fluid bilayers, shows a clear and statistically significant decrease in κ with increasing asymmetry in the range $8.6\% \leq \Delta n \leq 10.1\%$ (Fig. 5A and S4). This reduction in bending resistance is consistent with the behavior of K_A, confirming bilayer softening near the phase transition. A similar trend is observed using the TCB method, though the absolute values of κ are shifted. The observed pre-transition softening resembles the “anomalous swelling” phenomena reported in temperature-driven transitions by several experimental studies.(57-59)

The presence of curvature-sensitive inclusions in fluid membranes is known to induce softening, as described by the classic theory of Leibler.(60) This softening mechanism attributed to the coupling of curvature to membrane undulations has been supported by both computational and experimental studies.(61-63) Here, we approximate transient gel-like domains as a single curvature-sensitive inclusion of effective area A_G within an otherwise fluid bilayer, following the softening theory.(64) A prefactor of $1 / 2$ is applied to account for inclusion in a single leaflet. Under this assumption, the expected reduction in bending rigidity can be estimated as

$$\kappa_{apparent} \approx \kappa(1-\alpha)$$

with

$$\alpha = (\frac{1}{2})\frac{\kappa A_G(\Delta c_0^{gel})^2\chi(1-\chi)}{2k_BT}$$

Here, χ is the mole fraction of gel-like domains, A_G is the effective area of inclusion, and Δc_0^{gel} is the spontaneous curvature difference relative to the fluid background. For $\Delta n = 10.1\%$, we obtain $\chi = 0.22$, $\Delta c_0^{gel} = 0.012\ \mathrm{nm}^{-1}$, and $A_G = 57.9\ \mathrm{nm}^2$. Using the symmetric bilayer bending modulus $\kappa = 25.5\ k_B T$, this yields an estimated softening of only $\sim 1\%$. This prediction is, however, significantly smaller than the $\sim 16\%$ softening obtained directly from the hq method (Fig. 5A). It is important to note that the softening prediction is highly sensitive to Δc_0^{gel}, and small variations in curvature sampling can lead to substantial deviations from theoretical estimates. Nevertheless, we speculate that the additional reduction in apparent bending rigidity arises from enhanced bilayer dynamics associated with the continual formation and dissolution of gel-like domains in the pre-transition regime.

Asymmetry-induced phase behavior depends on lipid chemistry and force field. We assessed the generality of asymmetry-induced phase behavior by simulating additional systems, including coarse-grained (CG) DLPC bilayers using MARTINI 2.0, and an all-atom Lipid A bilayers (Tables S2-3). In all-atom Lipid A at 310 K, no phase transition occurred before reaching the bilayer's stress tolerance limit, beyond which bilayer integrity failed as the compressed leaflet expelled a lipid (Fig. S5). Further simulations showed a low T_m of ~290 K for Lipid A, making it unlikely that stress asymmetry would induce gel formation at physiological temperature (Fig. S6). By contrast, CG DLPC in MARTINI 2.0 did exhibit a fluid-to-gel phase transition when simulated at 300 K, close to its reported T_m.(65) Consistent changes in tail order parameter, area per lipid, and bilayer thickness (see Fig. 6A-C) indicated a transition at $\Delta n \approx 14\%$ (Fig. S7). This range is considerably higher than the $\approx 6\%$ reported phase transition limit by Ref. (31). The shift is attributable to the slightly elevated simulation temperature (+2.5 K) of this study and also the shorter 1.1 nm cutoff for Lennard-Jones and Coulomb interactions recommended in recent MARTINI protocols.

For DLPC, K_A increases sharply after gel formation (Fig. S8), consistent with the stiffening reported by Ref.(31) Moreover, both area compressibility and bending moduli show a softening trend near the transition threshold, accompanied by the formation of transient gel-like domains, consistent with our all-atom POPE results (Fig. 6D,E and S9). The apparent stiffening observed in bending modulus after gelation is expected thermodynamically but not quantitatively reliable, as computational methods to extract the bending modulus become impractical in the gel state (Fig. S2).

Extension to complex bacterial outer membrane systems. To evaluate asymmetry-driven structural responses beyond glycerophospholipid membranes, we simulated the outer membrane (OM) of *Pseudomonas aeruginosa* (*P. aeruginosa*) bacteria using all-atom molecular dynamics. The OM was composed of PA14 Lipid A in the outer leaflet and a mixture of POPE and 1-palmitoyl-2-oleoyl-sn-glycero-3-1-palmitoyl-2-oleoyl-sn-glycero-

3-phosphoglycerol (POPG) phospholipids (PLs) in the inner leaflet (Table S4). This system incorporates multiple relevant complexities, including compositional asymmetry, a multicomponent inner leaflet, charged lipids, and divalent cations that form ion bridges between Lipid A phosphate groups, making it a physiologically relevant testbed for our hypothesis.

Due to compositional asymmetry, the direction of asymmetry is important in this system. Asymmetry was parameterized relative to the membrane with minimum differential stress (0LT), generated using the zero-leaflet-tension method. We define asymmetry as:

$$r = n_i/n_o$$

$$\Delta n_r = \frac{r - r_{0LT}}{r_{0LT}}$$

where n_o and n_i are the number of lipids in the outer and inner leaflets, respectively, and r_{0LT} is the ratio in the zero differential stress state.(66) Positive Δn_r corresponds to inner leaflet compression (PLs leaflet), while negative Δn_r corresponds to outer leaflet compression (Lipid A leaflet). Table S6 shows a monotonic correlation between Δn_r and differential stress.

Consistent with our single-component results, compressing the outer leaflet (Lipid A) did not induce a phase transition, and this unique leaflet resisted compression until membrane integrity failed. In contrast, compressing the phospholipid inner leaflet ($\Delta n_r > +25\%$) led to the formation of ordered domains within the multicomponent PL leaflet. As shown in Fig. 7A-C, domain formation was accompanied by increased tail order parameter, decreased area per lipid, and locally high lipid packing (see Video S4). Similar to the simpler membranes, these ordered domains displayed curvature sensitivity, consistently residing in regions of positive curvature (Fig. 7D). These results demonstrate that asymmetry-driven domain formation and curvature preference, first observed in single-component bilayers, extend to multicomponent bacterial outer membranes, reinforcing the potential physiological relevance of this mechanism.

Discussion

Since the pioneering works of Bretscher (67) and Verkleij et al. (68) in the 1970s, membrane asymmetry has been recognized as a defining feature of biological membranes. Cells employ specialized transporter proteins known as flippases, floppases, and scramblases to control lipid asymmetry by actively translocating lipids between the two leaflets.(9, 69) Leaflet asymmetry can also arise from asymmetrically shaped transmembrane proteins, leaflet-specific lipid domains, or the anchoring of the cytoplasmic leaflet to submembrane networks such as the cytoskeleton or peptidoglycan layer.(11, 70) In addition to these compositional effects, cell membranes may also maintain number asymmetry, where the two leaflets contain unequal quantities of identical

lipids or molecules.(12, 71) This number asymmetry alters lipid packing and induces leaflet-specific strain, resulting in differential stress, a condition in which lateral tension differs between the two leaflets. Although differential stress is relatively easy to observe and control in computational modeling,(31, 66) direct experimental quantification remains challenging due to limitations in measuring microscopic stress in bilayers.(72) However, its effects can be inferred indirectly. For example, giant unilamellar vesicles (GUVs) are remarkably stable despite their low curvature, which is two orders of magnitude lower than the spontaneous curvature of their component lipids. Without invoking differential stress, there is no clear explanation for why the bending torque generated by their curvature does not induce tubulation. This likely differential stress has been estimated to be in the order of several mN/m.(73) Additionaly, differential stress has been predicted to influence several biological functions, including lipid flip-flop, membrane budding, activation of transmembrane proteins, peptide-induced pore formation, and the intercalation of small molecules.(12, 13, 15, 66, 74, 75)

Recent studies have shown that differential bilayer stress can actively promote phase transitions and enhance lateral heterogeneity.(31, 32) Near the main phase transition temperature T_m, compressive stress can drive lipid molecules into the gel state. Depending on the magnitude of the stress, these gel domains may coexist with fluid regions, forming a stable heterogeneous mixture.(33) The connection between mechanical stress and phase behavior suggests a regulatory mechanism by which cells can modulate membrane fluidity and permeability, thereby broadening the physiological significance of lipid asymmetry. In addition to mechanical stress, several other factors including temperature, cholesterol content, ion concentration, and membrane-associated proteins contribute to the modulation of membrane phase behavior.(17, 26, 29, 76) Notably, the spontaneous curvature of lipids has been hypothesized to correlate with lateral organization and the overall phase state of membranes.(77, 78) Supporting this idea, experiments on asymmetric POPE/POPC large unilamellar vesicles (LUVs) (79) have shown that POPE, which has a T_m of ~25 °C, undergoes a phase transition at 16 °C when placed in the inner leaflet, but at 20 °C when located in the outer leaflet. This upward shift is attributed to curvature-induced differential stress as POPE with negative spontaneous curvature is forced to adopt positive curvature when positioned in the outer leaflet. These observations underscore the role of curvature-induced stress in modulating phase behavior, a connection supported by our results. For the systems examined in this study, we find that within a given leaflet, gel domains preferentially localize to regions of positive curvature, while disordered fluid regions are enriched in negatively curved areas (Fig. 3 and 6D). This spatial preference is consistent with the increase in spontaneous curvature driven by the tight packing and ordering of hydrocarbon chains. Overall, the observed phase distribution illustrates a dynamic and reciprocal interplay between membrane curvature and lipid phase state. Such curvature-phase coupling may also

influence, or be influenced by, the localization and activity of curvature-sensing proteins, providing an additional feedback mechanism linking membrane structure to function.

Several independent experiments have reported higher bending rigidity in asymmetrical vesicles compared to their symmetrical counterparts.(80-83) Coarse-grained simulations have attributed this stiffening to differential stress,(31, 32, 84) which can push bilayers toward the gel phase when near T_m. Interestingly, a recent experiment reported asymmetry-induced stiffening even in the absence of notable differential stress, suggesting additional complexity.(80) It is important to recognize the limitations of current experimental techniques. Accurately determining leaflet asymmetry remains challenging, and the physical effects of chemical probes used in mechanical measurements are not yet fully understood.(85) Despite these uncertainties, the collective evidence clearly supports that asymmetry substantially influences membrane mechanical properties.

From a broader perspective, while gel phases exhibit rich physical properties and are commonly observed *in vitro* and *in silico*,(32, 33, 43, 86) their suppression of bilayer fluidity renders them largely incompatible with *in vivo* conditions, where dynamic membrane behavior is essential for cell function.(35, 36, 87) Our simulation snapshots display a dramatic loss of fluidity upon a fluid-to-gel phase transition, in agreement with previous literature.(88) Therefore, we argue that a more physiologically relevant regime lies just below the transition threshold, where the membrane is under differential stress, near T_m, but maintains a globally fluid state. A recent computational study reported a modest (<25%) increase in bending rigidity under asymmetry, even in the absence of visible lateral heterogeneity.(89) These systems were treated as homogeneous throughout the simulation. The explanation offered centered on the greater sensitivity of van der Waals forces to compression than extension, resulting in the compressed leaflet dominating bilayer mechanics. However, in our simulations, we do not observe statistically significant stiffening within the low asymmetry regime where the bilayer remains fluid.

Intriguingly, as the system approaches the transition threshold, we observe a reduction in both the area compressibility modulus and bending modulus, indicating a non-monotonic mechanical response to increasing asymmetry. This softened regime is characterized by enhanced lateral fluctuations, driven by the transient formation of ordered gel-like domains. These domains increase area oscillation, thereby reducing area compressibility modulus. Concurrently, curvature analysis reveals that gel domains localize in highly curved areas (Fig. 3 and 6D). The spontaneous appearance and disappearance of gel-like domains locally modulate curvature, contributing to a dynamic feedback that amplifies undulatory fluctuations. A similar curvature instability on a global scale has been observed in coarse-grained Monte Carlo simulations under conditions of phase coexistence.(84) The sensitivity of transient gel-like domains to curvature may be a key contributor to the softening effect we observe. Their formation promotes localized bending, and their

eventual dissolution relaxes curvature. This mechanism resonates with recent results from Ref. (90), where lipid mixtures with contrasting spontaneous curvatures induced membrane softening through nonadditive structural effects.(91, 92) However, curvature-composition coupling theory (60, 64) underestimates the degree of softening observed in our simulations. We speculate that the transient nature of gel-like domain formation introduces an additional dynamic mode of softening, whereby time-dependent recruitment and relaxation of curved domains amplifies membrane undulations. This interpretation aligns with Schick's theoretical framework,(93) in which curvature-composition coupling gives rise to transient "microemulsion" domains that reduce the bending energy of bilayer fluctuations, even in the absence of full phase separation. However, the underlying mechanisms of softening are likely more complex. Collective effects, such as inter-leaflet coupling, may further modulate membrane mechanics in the presence of asymmetric transient domains. Targeted investigations will be necessary to disentangle these contributions and clarify the origins of the softening observed in this regime. Finally, it is worth noting that enhanced bilayer fluctuations near phase transitions have also been observed experimentally.(37, 94) The reduction of bending rigidity in this regime is frequently associated with the phenomenon of anomalous swelling.(57-59)

One may question whether the observed softening near the transition is simply a consequence of bilayer thinning. While the polymer-brush model may not hold in this regime, we emphasize that the observed ~16% decrease in bending modulus and 36% decrease in compressibility modulus cannot be explained by the ~2% reduction in thickness. Another potential critique concerns the transient ordered domains "flakes" reported here, and whether they are simply part of natural fluctuations. However, our analysis shows that these domains can reach ~100 lipids in size and persist for over 100 ns, significantly larger and longer-lived than background fluctuations in symmetric bilayers (see Fig. 4B,C). One caveat of our study is the difficulty of sampling near phase transition regimes using all-atom force fields. Transient domain formation slows relaxation and increases autocorrelation times, requiring extended trajectories. Although we performed 2 μs equilibration followed by 2 μs analysis, longer simulations would likely provide more definitive evidence for the observed behavior. Additionally, it is important to note that the elastic moduli reported here represent global averages over the entire bilayer. This is a standard approach when analyzing fluid membranes. However, with the onset of gel-like domain formation, the mechanical properties of individual domains and leaflets will inevitably vary. Even so, the apparent average moduli remain informative and relevant to membrane shape remodeling.

To assess the generality of these findings, we extended our analysis to a bacterial outer membrane model that better reflects physiological complexity. Despite this system's increased compositional and structural complexities, we still observed a similar fluid-to-gel phase transition. This model, of course, introduces additional complications and

requires further study to be fully understood. For instance, the presence of divalent ion bridges in the outer leaflet (composed of Lipid A) likely increases its tolerance to negative differential stress, which results from crowding and compression of the inner PL leaflet. We acknowledge that including the full lipopolysaccharide structure instead of only the Lipid A anchor could potentially alter the observed behavior. However, the added sugars would likely increase the number of ion bridges, and thus could further enhance stress tolerance. Regardless, the key takeaway from this complex model is the plausibility of accessing the near-transition regime in a physiologically relevant context.

Our findings support and extend previous studies on the impact of asymmetry on membrane structure and function.(13, 31-33, 83) We propose that both eukaryotic and prokaryotic cells may use asymmetry as a regulatory mechanism to fine-tune their lateral phase behavior. This modulation could support various biological functions, including protein recruitment and activation, fluidity control, and defense against environmental stress. For instance, bacteria might exploit asymmetry-induced stiffening to resist antimicrobial peptides that disrupt membrane mechanics,(95) or induce softening to facilitate vesiculation.(96, 97)

Methods

All-atom MD simulations

All-atom simulations were conducted using the CHARMM36 force field.(98, 99) POPE bilayers contained only POPE lipids and water. Lipid A bilayers were composed of hexa-acylated *P. aeruginosa* Lipid A (PA14 strain), with calcium ions added for charge neutralization. The bacterial outer membrane (OM) model was constructed based on experimental lipidomics data,(100-102) with outer leaflet consisted of Lipid A, and the inner leaflet contained a 2.2:1 mixture of POPE and POPG. Sodium and calcium ions were introduced to neutralize the charges of POPG and Lipid A, respectively, and 150 mM NaCl was added to mimic physiological conditions. NBFIX (103, 104) corrections were applied to improve the accuracy of ion-lipid and ion-ion interactions.

Initial configurations were generated using the CHARMM-GUI membrane builder,(105) and simulations were carried out with GROMACS 2023.1.(106, 107) Each system underwent energy minimization via the steepest descent algorithm, followed by 100 ps of equilibration under an NVT ensemble using the velocity-rescaling thermostat,(108) with separate coupling for lipids and solvent. Production simulations were then performed in the NPT ensemble using semi-isotropic pressure coupling at 1 bar, combining stochastic cell rescaling barostat (109) and stochastic velocity rescaling thermostat.(110) Equilibration durations ranged from 2 to 5 μs. All bonds involving hydrogen atoms were constrained using the LINCS algorithm.(111) Short-range van der Waals and electrostatic interactions were truncated at 1.2 nm, with neighbor lists updated every 20 steps. Long-range electrostatics were treated using the Particle-Mesh Ewald (PME) method.(112) A 2

fs integration timestep was used with the leapfrog integrator. Detailed simulation parameters, system compositions, and data sampling information are provided in Supporting Information (SI).

Coarse-grained MD simulations

Coarse-grained simulations were performed using the MARTINI 2.0 force field.(113) A timestep of 20 fs was employed. Following established protocols, Lennard-Jones and Coulomb interactions were truncated at 1.1 nm, and a relative dielectric constant of 15 was used. Thermostats and barostats were implemented using stochastic velocity rescaling and stochastic cell rescaling, respectively. Neighbor list parameters were set according to the recommendations in Ref. (114).

Hidden Markov Model

Gaussian Hidden Markov Model (GHMM) was used to assign lipid phase states based on per-lipid structural features. A two-state GHMM was implemented to represent ordered and disordered phases. Features included area per lipid, carbon-carbon order parameter, and tail height. Initial emission distributions were estimated by fitting a Gaussian Mixture Model (GMM) to a system exhibiting clear phase separation. The GHMM was then trained using the Viterbi algorithm.(115) To ensure robustness against local minima, the model was trained under 10 different random seeds, and the one with the highest log-likelihood was selected. GMM and GHMM analyses were performed using the scikit-learn and hmmlearn Python packages, respectively.

Acknowledgments

We thank Alexander Sodt for assistance in MembraneAnalysis.jl package, constructive discussion, and critical reading of the manuscript. This work was supported in part by U.S. National Science Foundation grant #2448213 and National Institutes of Health grant 1R15GM135862. Computational resources of this research were provided by the Center for Computational Research at the University at Buffalo and allocation BIO220055 from the Advanced Cyberinfrastructure Coordination Ecosystem: Services & Support (ACCESS) program, which is supported by U.S. National Science Foundation grants #2138259, #2138286, #2138307, #2137603, and #2138296.

References

1. K. Simons, D. Toomre, Lipid rafts and signal transduction. *Nat Rev Mol Cell Biol* **1**, 31-39 (2000).
2. S. J. Singer, G. L. Nicolson, The fluid mosaic model of the structure of cell membranes. *Science* **175**, 720-731 (1972).
3. H. G. Dobereiner, J. Kas, D. Noppl, I. Sprenger, E. Sackmann, Budding and fission of vesicles. *Biophys J* **65**, 1396-1403 (1993).

4. G. van Meer, D. R. Voelker, G. W. Feigenson, Membrane lipids: where they are and how they behave. *Nat Rev Mol Cell Biol* **9**, 112-124 (2008).
5. D. Lingwood, K. Simons, Lipid rafts as a membrane-organizing principle. *Science* **327**, 46-50 (2010).
6. F. X. Contreras, L. Sanchez-Magraner, A. Alonso, F. M. Goni, Transbilayer (flip-flop) lipid motion and lipid scrambling in membranes. *FEBS Lett* **584**, 1779-1786 (2010).
7. T. A. Enoki, F. A. Heberle, Experimentally determined leaflet-leaflet phase diagram of an asymmetric lipid bilayer. *Proc Natl Acad Sci U S A* **120**, e2308723120 (2023).
8. J. H. Lorent *et al.*, Plasma membranes are asymmetric in lipid unsaturation, packing and protein shape. *Nat Chem Biol* **16**, 644-652 (2020).
9. S. Nagata, T. Sakuragi, K. Segawa, Flippase and scramblase for phosphatidylserine exposure. *Curr Opin Immunol* **62**, 31-38 (2020).
10. J. I. Elliott *et al.*, Membrane phosphatidylserine distribution as a non-apoptotic signalling mechanism in lymphocytes. *Nat Cell Biol* **7**, 808-816 (2005).
11. M. Doktorova, J. L. Symons, I. Levental, Structural and functional consequences of reversible lipid asymmetry in living membranes. *Nat Chem Biol* **16**, 1321-1330 (2020).
12. B. Rozycki, R. Lipowsky, Spontaneous curvature of bilayer membranes from molecular simulations: asymmetric lipid densities and asymmetric adsorption. *J Chem Phys* **142**, 054101 (2015).
13. P. Piller, E. F. Semeraro, G. N. Rechberger, S. Keller, G. Pabst, Allosteric modulation of integral protein activity by differential stress in asymmetric membranes. *PNAS Nexus* **2**, pgad126 (2023).
14. H. T. McMahon, J. L. Gallop, Membrane curvature and mechanisms of dynamic cell membrane remodelling. *Nature* **438**, 590-596 (2005).
15. G. S. Attard, R. H. Templer, W. S. Smith, A. N. Hunt, S. Jackowski, Modulation of CTP:phosphocholine cytidylyltransferase by membrane curvature elastic stress. *Proc Natl Acad Sci U S A* **97**, 9032-9036 (2000).
16. H. Y. Wang *et al.*, Loss of lipid asymmetry facilitates plasma membrane blebbing by decreasing membrane lipid packing. *Proc Natl Acad Sci U S A* **122**, e2417145122 (2025).
17. J. B. Larsen *et al.*, Membrane curvature enables N-Ras lipid anchor sorting to liquid-ordered membrane phases. *Nat Chem Biol* **11**, 192-194 (2015).
18. J. Bigay, B. Antonny, Curvature, lipid packing, and electrostatics of membrane organelles: defining cellular territories in determining specificity. *Dev Cell* **23**, 886-895 (2012).
19. K. Simons, E. Ikonen, Functional rafts in cell membranes. *Nature* **387**, 569-572 (1997).
20. S. A. Shelby, I. Castello-Serrano, K. C. Wisser, I. Levental, S. L. Veatch, Membrane phase separation drives responsive assembly of receptor signaling domains. *Nat Chem Biol* **19**, 750-758 (2023).
21. M. Heinrich, A. Tian, C. Esposito, T. Baumgart, Dynamic sorting of lipids and proteins in membrane tubes with a moving phase boundary. *Proc Natl Acad Sci U S A* **107**, 7208-7213 (2010).

22. T. Baumgart *et al.*, Large-scale fluid/fluid phase separation of proteins and lipids in giant plasma membrane vesicles. *Proc Natl Acad Sci U S A* **104**, 3165-3170 (2007).
23. S. L. Veatch, S. L. Keller, Separation of liquid phases in giant vesicles of ternary mixtures of phospholipids and cholesterol. *Biophys J* **85**, 3074-3083 (2003).
24. R. F. de Almeida, L. M. Loura, A. Fedorov, M. Prieto, Nonequilibrium phenomena in the phase separation of a two-component lipid bilayer. *Biophys J* **82**, 823-834 (2002).
25. I. Levental, K. R. Levental, F. A. Heberle, Lipid Rafts: Controversies Resolved, Mysteries Remain. *Trends Cell Biol* **30**, 341-353 (2020).
26. I. Levental *et al.*, Cholesterol-dependent phase separation in cell-derived giant plasma-membrane vesicles. *Biochem J* **424**, 163-167 (2009).
27. J. H. Ipsen, G. Karlstrom, O. G. Mouritsen, H. Wennerstrom, M. J. Zuckermann, Phase equilibria in the phosphatidylcholine-cholesterol system. *Biochim Biophys Acta* **905**, 162-172 (1987).
28. J. Korlach, P. Schwille, W. W. Webb, G. W. Feigenson, Characterization of lipid bilayer phases by confocal microscopy and fluorescence correlation spectroscopy. *Proc Natl Acad Sci U S A* **96**, 8461-8466 (1999).
29. D. Chapman, Phase transitions and fluidity characteristics of lipids and cell membranes. *Q Rev Biophys* **8**, 185-235 (1975).
30. J. Pan, S. Tristram-Nagle, N. Kucerka, J. F. Nagle, Temperature dependence of structure, bending rigidity, and bilayer interactions of dioleoylphosphatidylcholine bilayers. *Biophys J* **94**, 117-124 (2008).
31. A. Hossein, M. Deserno, Spontaneous Curvature, Differential Stress, and Bending Modulus of Asymmetric Lipid Membranes. *Biophys J* **118**, 624-642 (2020).
32. A. Hossein, M. Deserno, Stiffening transition in asymmetric lipid bilayers: The role of highly ordered domains and the effect of temperature and size. *J Chem Phys* **154**, 014704 (2021).
33. S. L. Foley, A. Hossein, M. Deserno, Fluid-gel coexistence in lipid membranes under differential stress. *Biophys J* **121**, 2997-3009 (2022).
34. F. A. Heberle, G. W. Feigenson, Phase separation in lipid membranes. *Cold Spring Harb Perspect Biol* **3** (2011).
35. J. R. Hazel, Thermal adaptation in biological membranes: is homeoviscous adaptation the explanation? *Annu Rev Physiol* **57**, 19-42 (1995).
36. E. Z. Drobnis *et al.*, Cold shock damage is due to lipid phase transitions in cell membranes: a demonstration using sperm as a model. *J Exp Zool* **265**, 432-437 (1993).
37. S. L. Veatch *et al.*, Critical fluctuations in plasma membrane vesicles. *ACS Chem Biol* **3**, 287-293 (2008).
38. M. Burns, K. Wisser, J. Wu, I. Levental, S. L. Veatch, Miscibility Transition Temperature Scales with Growth Temperature in a Zebrafish Cell Line. *Biophys J* **113**, 1212-1222 (2017).
39. A. Sarra *et al.*, Biophysical Characterization of Membrane Phase Transition Profiles for the Discrimination of Outer Membrane Vesicles (OMVs) From Escherichia coli Grown at Different Temperatures. *Front Microbiol* **11**, 290 (2020).

40. K. Emoto *et al.*, Redistribution of phosphatidylethanolamine at the cleavage furrow of dividing cells during cytokinesis. *Proc Natl Acad Sci U S A* **93**, 12867-12872 (1996).
41. A. Irie, K. Yamamoto, Y. Miki, M. Murakami, Phosphatidylethanolamine dynamics are required for osteoclast fusion. *Sci Rep* **7**, 46715 (2017).
42. W. Dowhan, Molecular basis for membrane phospholipid diversity: why are there so many lipids? *Annu Rev Biochem* **66**, 199-232 (1997).
43. J. F. Nagle, S. Tristram-Nagle, Structure of lipid bilayers. *Biochim Biophys Acta* **1469**, 159-195 (2000).
44. K. C. Sapp, A. H. Beaven, A. J. Sodt, Spatial extent of a single lipid's influence on bilayer mechanics. *Phys Rev E* **103**, 042413 (2021).
45. A. Hossein, A. J. Sodt, MembraneAnalysis.jl: A Julia package for analyzing molecular dynamics simulations of lipid membranes. *Journal of Open Source Software* **8** (2023).
46. L. E. Baum, T. Petrie, Statistical Inference for Probabilistic Functions of Finite State Markov Chains. *The Annals of Mathematical Statistics* **37**, 1554-1563 (1966).
47. M. F. W. Trollmann, R. A. Bockmann, Characterization of domain formation in complex membranes. *Methods Enzymol* **701**, 1-46 (2024).
48. A. J. Sodt, M. L. Sandar, K. Gawrisch, R. W. Pastor, E. Lyman, The molecular structure of the liquid-ordered phase of lipid bilayers. *J Am Chem Soc* **136**, 725-732 (2014).
49. S. E. Feller, R. W. Pastor, Constant surface tension simulations of lipid bilayers: The sensitivity of surface areas and compressibilities. *The Journal of Chemical Physics* **111**, 1281-1287 (1999).
50. M. M. Terzi, M. Deserno, Novel tilt-curvature coupling in lipid membranes. *J Chem Phys* **147**, 084702 (2017).
51. R. Goetz, G. Gompper, R. Lipowsky, Mobility and Elasticity of Self-Assembled Membranes. *Physical Review Letters* **82**, 221-224 (1999).
52. M. Doktorova, D. Harries, G. Khelashvili, Determination of bending rigidity and tilt modulus of lipid membranes from real-space fluctuation analysis of molecular dynamics simulations. *Phys Chem Chem Phys* **19**, 16806-16818 (2017).
53. G. Khelashvili, B. Kollmitzer, P. Heftberger, G. Pabst, D. Harries, Calculating the Bending Modulus for Multicomponent Lipid Membranes in Different Thermodynamic Phases. *J Chem Theory Comput* **9**, 3866-3871 (2013).
54. M. Hamm, M. M. Kozlov, Elastic energy of tilt and bending of fluid membranes. *The European Physical Journal E* **3**, 323-335 (2000).
55. H. Noguchi, Anisotropic surface tension of buckled fluid membranes. *Phys Rev E Stat Nonlin Soft Matter Phys* **83**, 061919 (2011).
56. M. Hu, P. Diggins, M. Deserno, Determining the bending modulus of a lipid membrane by simulating buckling. *J Chem Phys* **138**, 214110 (2013).
57. E. G. Kelley, M. Nagao, P. D. Butler, L. Porcar, B. Farago, Enhanced dynamics in the anomalous melting regime of DMPG lipid membranes. *Struct Dyn* **7**, 054704 (2020).
58. P. Meleard *et al.*, Bending elasticities of model membranes: influences of temperature and sterol content. *Biophys J* **72**, 2616-2629 (1997).

59. N. Chu, N. Kucerka, Y. Liu, S. Tristram-Nagle, J. F. Nagle, Anomalous swelling of lipid bilayer stacks is caused by softening of the bending modulus. *Phys Rev E Stat Nonlin Soft Matter Phys* **71**, 041904 (2005).
60. S. Leibler, Curvature instability in membranes. *Journal de Physique* **47**, 507-516 (1986).
61. M. M. Kozlov, W. Helfrich, Effects of a cosurfactant on the stretching and bending elasticities of a surfactant monolayer. *Langmuir* **8**, 2792-2797 (2002).
62. K. Sapp, M. Aleksanyan, K. Kerr, R. Dimova, A. Sodt, Kinetic relaxation of giant vesicles validates diffusional softening in a binary lipid mixture. *Phys Rev E* **107**, 054403 (2023).
63. P. V. Bashkirov, K. V. Chekashkina, S. A. Akimov, P. I. Kuzmin, V. A. Frolov, Variation of lipid membrane composition caused by strong bending. *Biochemistry (Moscow) Supplement Series A: Membrane and Cell Biology* **5**, 205-211 (2011).
64. P. V. Bashkirov, P. I. Kuzmin, J. Vera Lillo, V. A. Frolov, Molecular Shape Solution for Mesoscopic Remodeling of Cellular Membranes. *Annu Rev Biophys* **51**, 473-497 (2022).
65. J. M. Rodgers, J. Sorensen, F. J. de Meyer, B. Schiott, B. Smit, Understanding the phase behavior of coarse-grained model lipid bilayers through computational calorimetry. *J Phys Chem B* **116**, 1551-1569 (2012).
66. E. Pirhadi, J. M. Vanegas, M. Farin, J. W. Schertzer, X. Yong, Effect of Local Stress on Accurate Modeling of Bacterial Outer Membranes Using All-Atom Molecular Dynamics. *J Chem Theory Comput* **19**, 363-372 (2023).
67. M. S. Bretscher, Asymmetrical lipid bilayer structure for biological membranes. *Nat New Biol* **236**, 11-12 (1972).
68. A. J. Verkleij *et al.*, The asymmetric distribution of phospholipids in the human red cell membrane. A combined study using phospholipases and freeze-etch electron microscopy. *Biochim Biophys Acta* **323**, 178-193 (1973).
69. T. Pomorski, A. K. Menon, Lipid flippases and their biological functions. *Cell Mol Life Sci* **63**, 2908-2921 (2006).
70. M. P. Sheetz, Cell control by membrane-cytoskeleton adhesion. *Nat Rev Mol Cell Biol* **2**, 392-396 (2001).
71. M. Doktorova *et al.*, Cell membranes sustain phospholipid imbalance via cholesterol asymmetry. *Cell* **188**, 2586-2602 e2524 (2025).
72. T. Reagle, Y. Xie, Z. Li, W. Carnero, T. Baumgart, Methyl-beta-cyclodextrin asymmetrically extracts phospholipid from bilayers, granting tunable control over differential stress in lipid vesicles. *Soft Matter* **20**, 4291-4307 (2024).
73. M. Deserno, Biomembranes balance many types of leaflet asymmetries. *Curr Opin Struct Biol* **87**, 102832 (2024).
74. M. Krompers *et al.*, Asymmetric phase transitions in lipid bilayers: coupling or bending? *Faraday Discuss* **259**, 107-128 (2025).
75. A. Rice, A. C. Zourou, M. L. Cotten, R. W. Pastor, A unified model of transient poration induced by antimicrobial peptides. *Proc Natl Acad Sci U S A* **122**, e2510294122 (2025).
76. H. Trauble, H. Eibl, Electrostatic effects on lipid phase transitions: membrane structure and ionic environment. *Proc Natl Acad Sci U S A* **71**, 214-219 (1974).

77. A. Buyan, D. W. Allender, B. Corry, M. Schick, Lipid redistribution in the highly curved footprint of Piezo1. *Biophys J* **122**, 1900-1913 (2023).
78. D. W. Allender, A. J. Sodt, M. Schick, Cholesterol-Dependent Bending Energy Is Important in Cholesterol Distribution of the Plasma Membrane. *Biophys J* **116**, 2356-2366 (2019).
79. B. Eicher *et al.*, Intrinsic Curvature-Mediated Transbilayer Coupling in Asymmetric Lipid Vesicles. *Biophys J* **114**, 146-157 (2018).
80. M. P. K. Frewein *et al.*, Distributing aminophospholipids asymmetrically across leaflets causes anomalous membrane stiffening. *Biophys J* **122**, 2445-2455 (2023).
81. B. W. Rickeard *et al.*, Transverse lipid organization dictates bending fluctuations in model plasma membranes. *Nanoscale* **12**, 1438-1447 (2020).
82. L. Lu, W. J. Doak, J. W. Schertzer, P. R. Chiarot, Membrane mechanical properties of synthetic asymmetric phospholipid vesicles. *Soft Matter* **12**, 7521-7528 (2016).
83. Y. Elani *et al.*, Measurements of the effect of membrane asymmetry on the mechanical properties of lipid bilayers. *Chem Commun (Camb)* **51**, 6976-6979 (2015).
84. O. Farago, Measuring the mechanical properties of asymmetric membranes in computer simulations - new methods and insights. *Faraday Discuss* **259**, 321-341 (2025).
85. D. Drabik *et al.*, Effect of leaflet asymmetry on the stretching elasticity of lipid bilayers with phosphatidic acid. *Biophys J* **123**, 2406-2421 (2024).
86. R. Dimova, B. Pouligny, C. Dietrich, Pretransitional effects in dimyristoylphosphatidylcholine vesicle membranes: optical dynamometry study. *Biophys J* **79**, 340-356 (2000).
87. K. Simons, W. L. Vaz, Model systems, lipid rafts, and cell membranes. *Annu Rev Biophys Biomol Struct* **33**, 269-295 (2004).
88. A. Kumar, S. Daschakraborty, Anomalous lateral diffusion of lipids during the fluid/gel phase transition of a lipid membrane. *Phys Chem Chem Phys* **25**, 31431-31443 (2023).
89. G. Fiorin, L. R. Forrest, Elucidating the mechanical properties of asymmetric membranes by direct derivation of their energetics. *Faraday Discuss* **259**, 437-453 (2025).
90. A. Hossein, A. H. Beaven, K. Sapp, A. J. Sodt, Softening in Two-Component Lipid Mixtures by Spontaneous Curvature Variance. *J Phys Chem B* **128**, 6317-6326 (2024).
91. A. J. Sodt, R. M. Venable, E. Lyman, R. W. Pastor, Nonadditive Compositional Curvature Energetics of Lipid Bilayers. *Phys Rev Lett* **117**, 138104 (2016).
92. E. G. Kelley, P. D. Butler, R. Ashkar, R. Bradbury, M. Nagao, Scaling relationships for the elastic moduli and viscosity of mixed lipid membranes. *Proc Natl Acad Sci U S A* **117**, 23365-23373 (2020).
93. M. Schick, Membrane heterogeneity: manifestation of a curvature-induced microemulsion. *Phys Rev E Stat Nonlin Soft Matter Phys* **85**, 031902 (2012).
94. R. Dimova, Recent developments in the field of bending rigidity measurements on membranes. *Adv Colloid Interface Sci* **208**, 225-234 (2014).

95. S. Omardien *et al.*, Bactericidal activity of amphipathic cationic antimicrobial peptides involves altering the membrane fluidity when interacting with the phospholipid bilayer. *Biochim Biophys Acta Biomembr* **1860**, 2404-2415 (2018).
96. C. Schwechheimer, M. J. Kuehn, Outer-membrane vesicles from Gram-negative bacteria: biogenesis and functions. *Nat Rev Microbiol* **13**, 605-619 (2015).
97. C. Gopal *et al.*, Membrane Stress Enhances Specific PQS–Lipid Interactions That Drive Bacterial Outer Membrane Vesicle Biogenesis. *Membranes* **15** (2025).
98. J. B. Klauda *et al.*, Update of the CHARMM all-atom additive force field for lipids: validation on six lipid types. *J Phys Chem B* **114**, 7830-7843 (2010).
99. K. Vanommeslaeghe, A. D. MacKerell, Jr., CHARMM additive and polarizable force fields for biophysics and computer-aided drug design. *Biochim Biophys Acta* **1850**, 861-871 (2015).
100. H. Benamara *et al.*, Characterization of membrane lipidome changes in Pseudomonas aeruginosa during biofilm growth on glass wool. *PLoS One* **9**, e108478 (2014).
101. Y. Tashiro *et al.*, Characterization of phospholipids in membrane vesicles derived from Pseudomonas aeruginosa. *Biosci Biotechnol Biochem* **75**, 605-607 (2011).
102. J. Chao, G. M. Wolfaardt, M. T. Arts, Characterization of Pseudomonas aeruginosa fatty acid profiles in biofilms and batch planktonic cultures. *Can J Microbiol* **56**, 1028-1039 (2010).
103. S. Kim *et al.*, Bilayer Properties of Lipid A from Various Gram-Negative Bacteria. *Biophys J* **111**, 1750-1760 (2016).
104. J. Yoo, A. Aksimentiev, Improved Parametrization of Li+, Na+, K+, and Mg2+ Ions for All-Atom Molecular Dynamics Simulations of Nucleic Acid Systems. *The Journal of Physical Chemistry Letters* **3**, 45-50 (2011).
105. S. Jo, T. Kim, V. G. Iyer, W. Im, CHARMM-GUI: a web-based graphical user interface for CHARMM. *J Comput Chem* **29**, 1859-1865 (2008).
106. H. J. C. Berendsen, D. van der Spoel, R. van Drunen, GROMACS: A message-passing parallel molecular dynamics implementation. *Computer Physics Communications* **91**, 43-56 (1995).
107. M. J. Abraham *et al.*, GROMACS: High performance molecular simulations through multi-level parallelism from laptops to supercomputers. *SoftwareX* **1-2**, 19-25 (2015).
108. L. V. Woodcock, Isothermal molecular dynamics calculations for liquid salts. *Chemical Physics Letters* **10**, 257-261 (1971).
109. M. Bernetti, G. Bussi, Pressure control using stochastic cell rescaling. *J Chem Phys* **153**, 114107 (2020).
110. G. Bussi, D. Donadio, M. Parrinello, Canonical sampling through velocity rescaling. *J Chem Phys* **126**, 014101 (2007).
111. B. Hess, P-LINCS: A Parallel Linear Constraint Solver for Molecular Simulation. *J Chem Theory Comput* **4**, 116-122 (2008).
112. T. Darden, D. York, L. Pedersen, Particle mesh Ewald: An N·log(N) method for Ewald sums in large systems. *The Journal of Chemical Physics* **98**, 10089-10092 (1993).

113. S. J. Marrink, H. J. Risselada, S. Yefimov, D. P. Tieleman, A. H. de Vries, The MARTINI force field: coarse grained model for biomolecular simulations. *J Phys Chem B* **111**, 7812-7824 (2007).
114. H. Kim, B. Fabian, G. Hummer, Neighbor List Artifacts in Molecular Dynamics Simulations. *J Chem Theory Comput* **19**, 8919-8929 (2023).
115. A. Viterbi, Error bounds for convolutional codes and an asymptotically optimum decoding algorithm. *IEEE Transactions on Information Theory* **13**, 260-269 (1967).

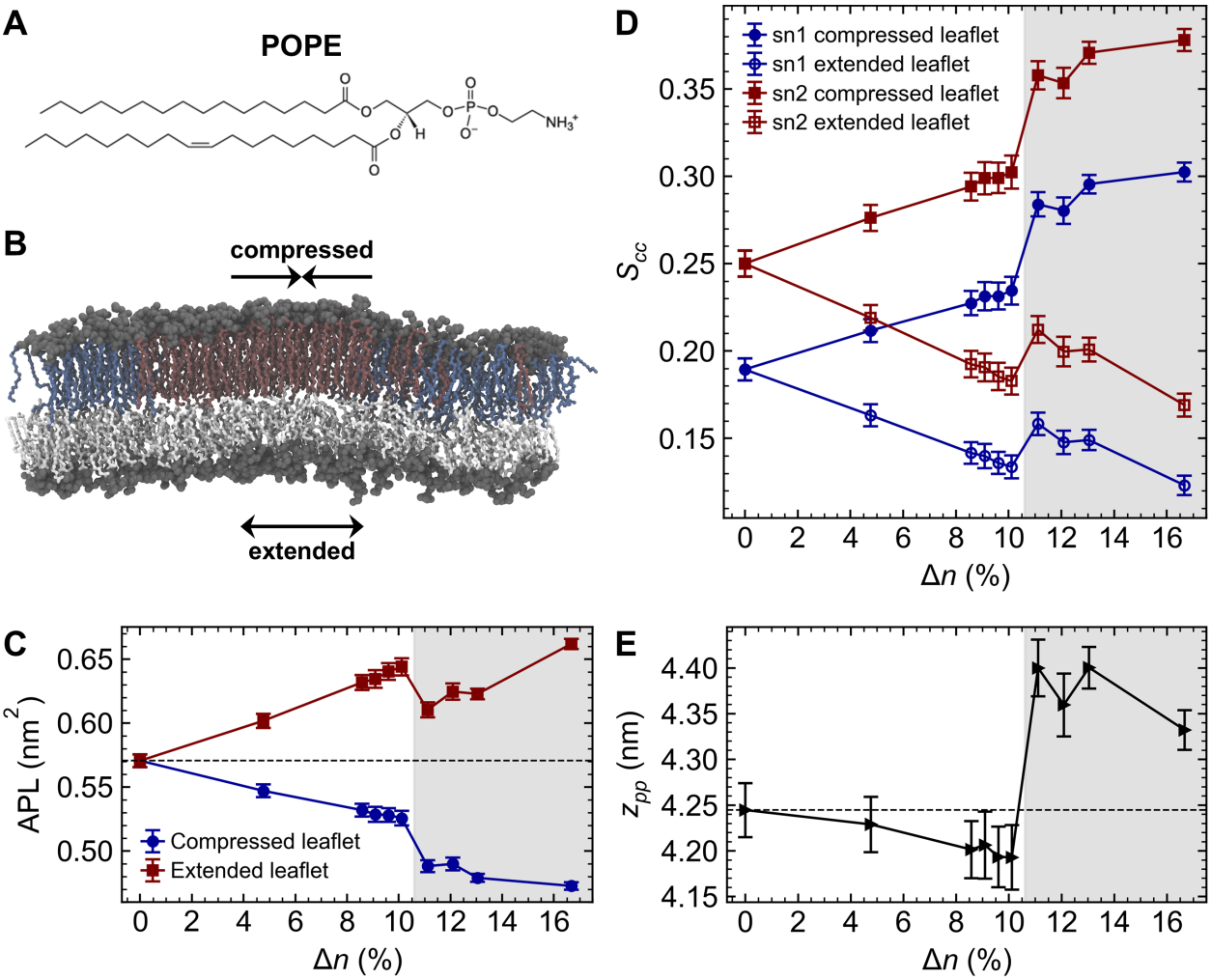

Figure 1. Stress asymmetry drives phase transition. (A) Chemical structure of POPE. (B) Representative simulation snapshot of a POPE bilayer under number asymmetry ($\Delta n \approx 13.0\%$). Lipid tails in the extended leaflet are shown in white, while lipid tails in the compressed leaflet are colored by phase: gel phase (dark red) and fluid phase (blue). (C) Area per lipid of each leaflet, (D) carbon-carbon order parameter per leaflet, and (E) phosphate-to-phosphate membrane thickness as functions of number asymmetry. Shaded regions indicate the post phase transition regime. Error bars represent standard deviations of the mean over time.

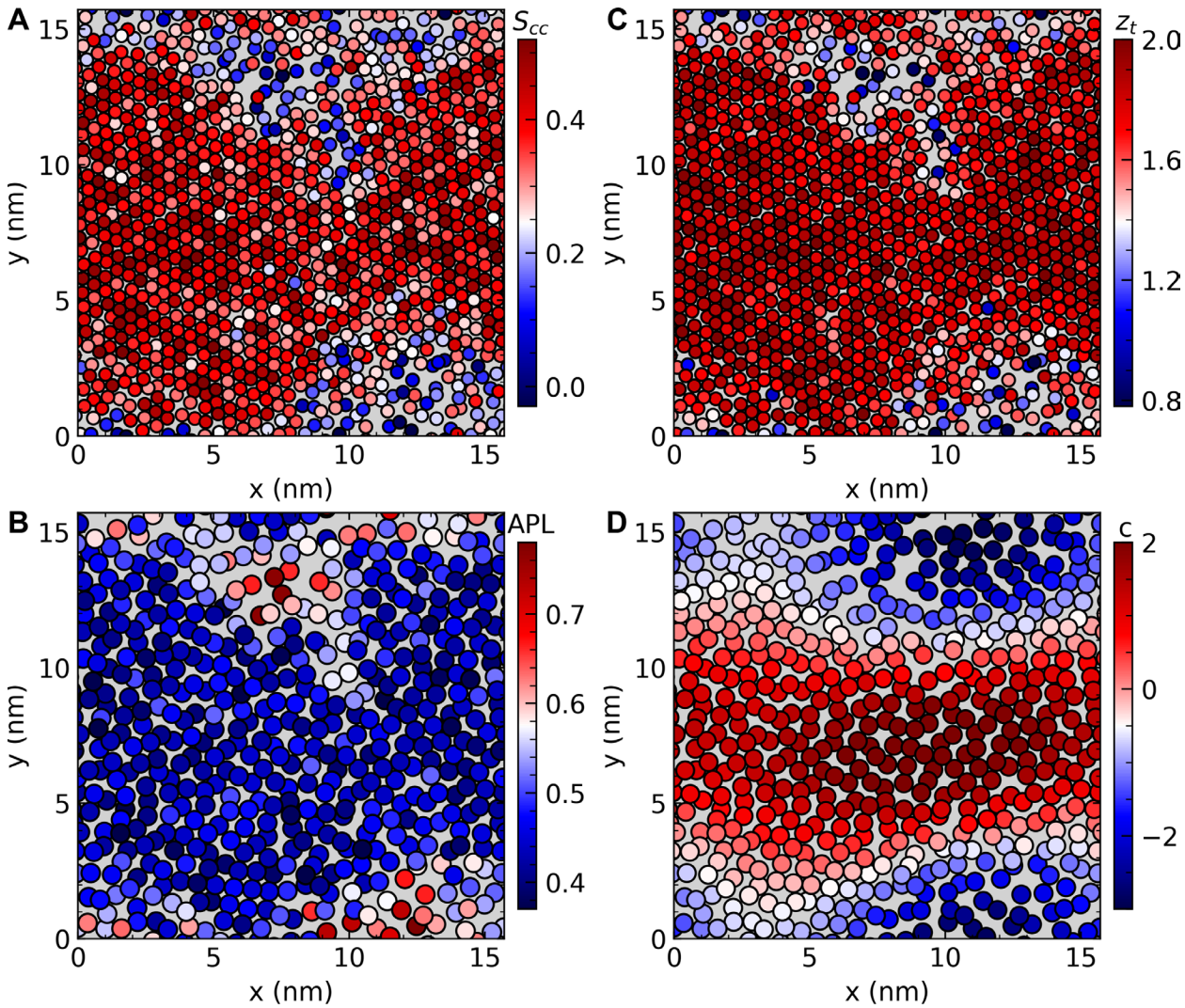

Figure 2. Stress asymmetry induces lateral phase separation. Heatmaps of structural properties for the compressed leaflet of a POPE membrane under number asymmetry of $\Delta n \approx 13.0\%$, plotted for the final simulation snapshot: (A) carbon-carbon order parameter, (B) tail height in the z-direction, (C) area per lipid, and (D) curvature experienced by each lipid. Each bead corresponds to (A,B) the center of mass of an individual lipid tail or (C,D) the average center of mass of both tails.

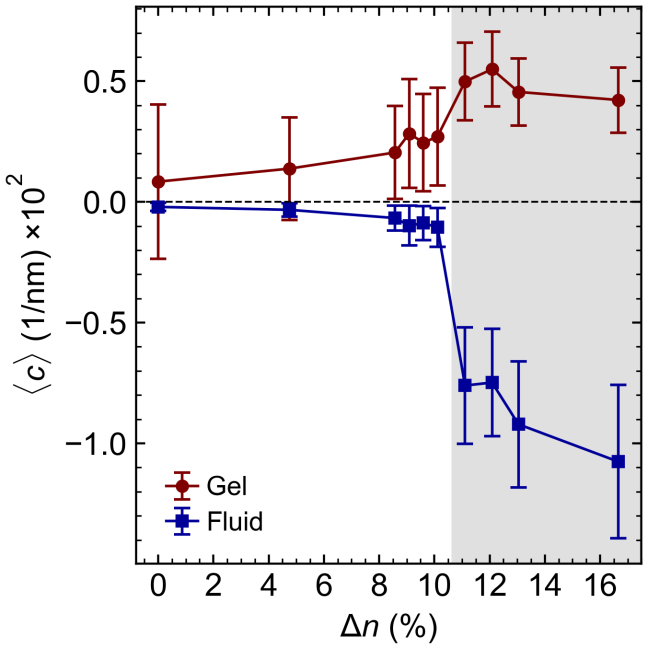

Figure 3. Lipid phase state modulates curvature preference. Time-averaged local curvature experienced by fluid and gel phase lipids in the compressed leaflet of POPE membranes, plotted as a function of number asymmetry. The shaded region marks the post phase transition regime. Error bars represent standard deviations of the mean over time.

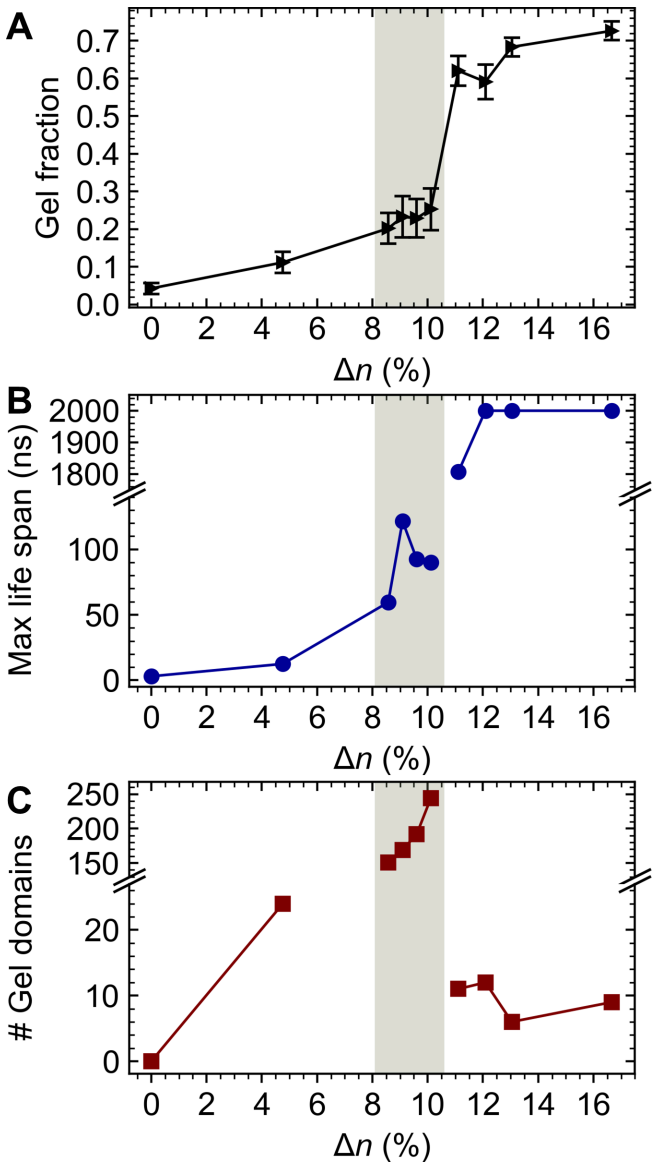

Figure 4. Asymmetry promotes transient gel-like domain formation near the transition threshold. (A) Fraction of gel-phase lipids in the compressed leaflet of POPE membranes, (B) maximal lifetime of gel clusters during the 2-μs simulation, and (C) total number of gel domains formed throughout the trajectory as functions of number asymmetry. Shaded areas highlight the near-transition regime exhibiting notable transient gel-like domains. Error bars denote standard deviations of the mean over time.

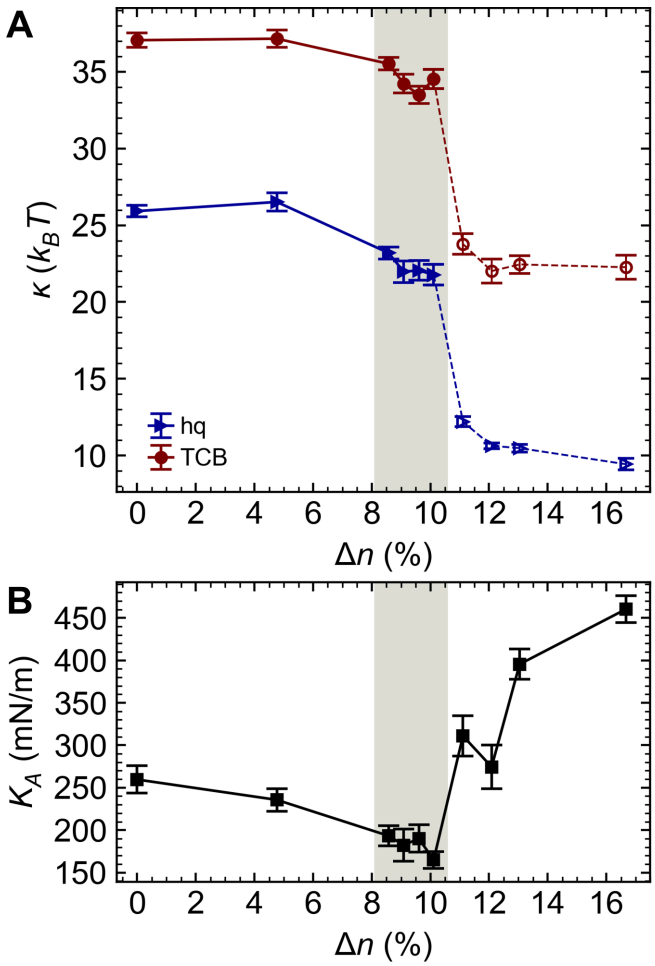

Figure 5. Membrane softening near the phase transition threshold. (A) Bending modulus and (B) area compressibility modulus plotted as functions of number asymmetry. Error bars represent standard errors of the mean obtained via block averaging (see SI for details). Shaded areas highlight the near-transition regime which exhibits notable transient gel-like domains.

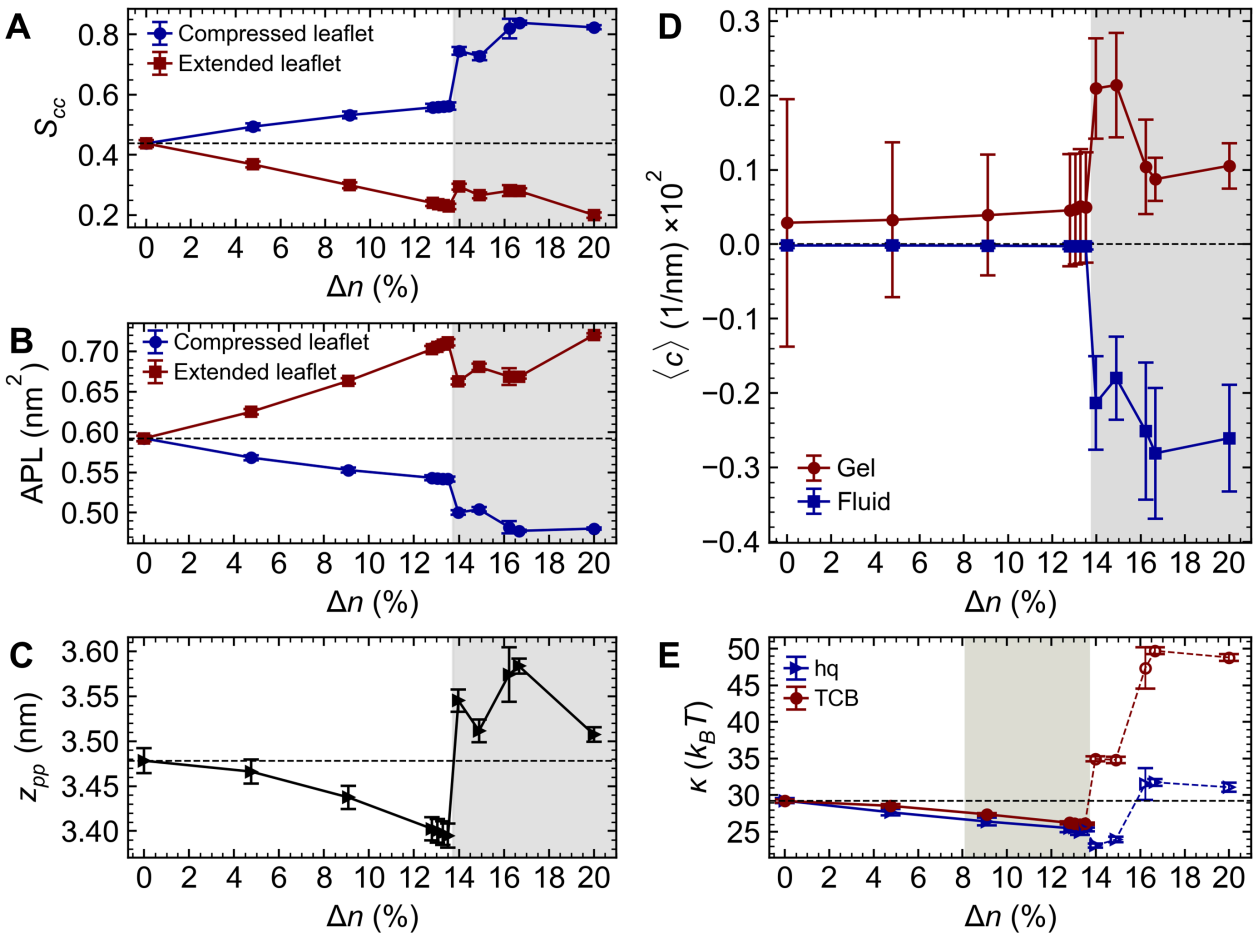

Figure 6. Softening near the transition regime in coarse-grained DLPC membranes. (A) Carbon-carbon order parameter, (B) area per lipid, (C) phosphate-to-phosphate membrane thickness, (D) time-averaged local curvature experienced by fluid and gel phase lipids, and (E) bending modulus as functions of number asymmetry. For panels A–D, error bars represent standard deviations over time; shaded regions indicate the onset of phase transition. In panel E, error bars show the standard error of the mean from block averaging; the shaded region denotes the near-transition regime.

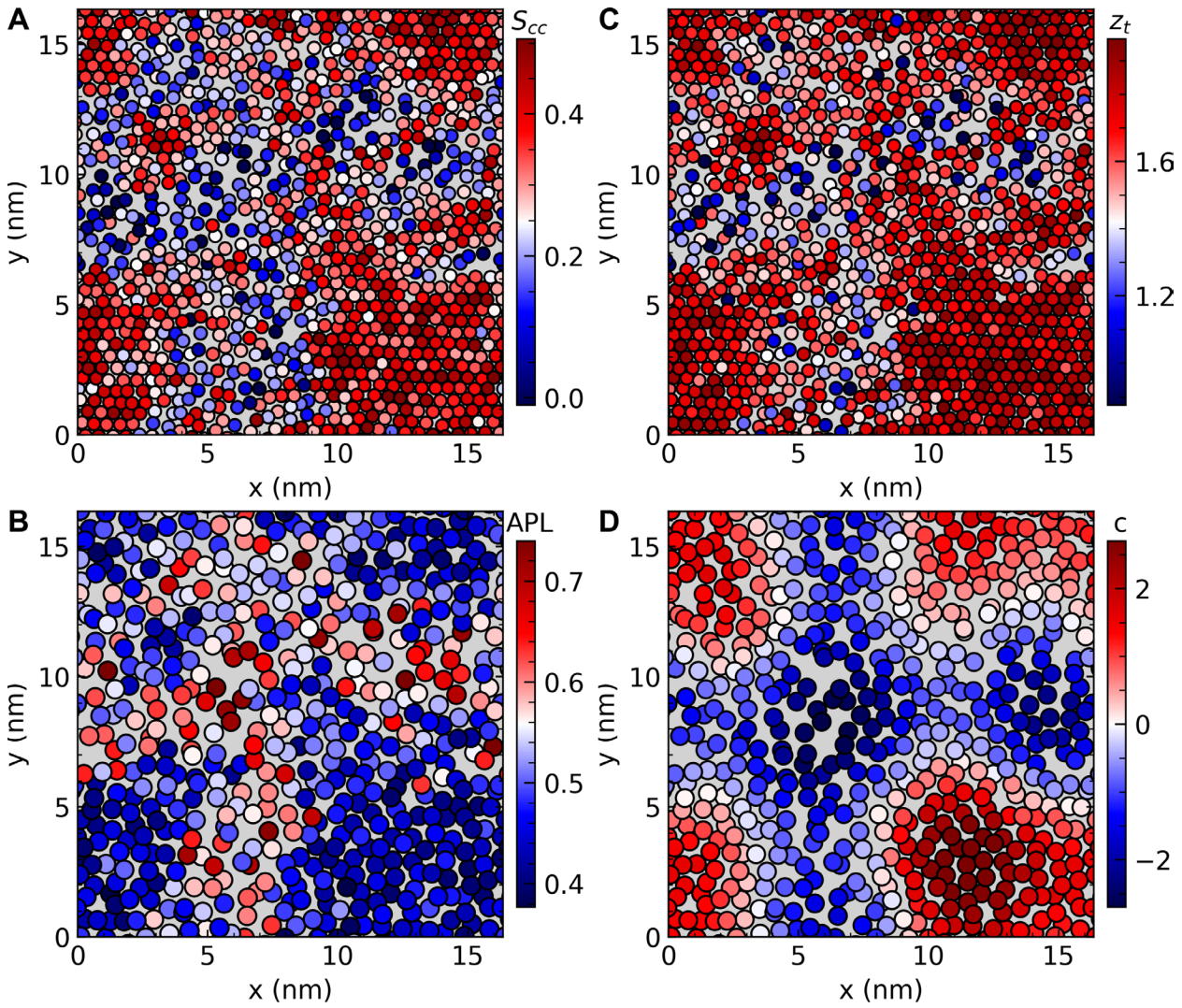

Figure 7. Stress asymmetry drives phase transition in the PLs leaflet of the OM. Heatmaps of structural properties for the compressed (PLs) leaflet under relative number asymmetry of $\Delta n_r \approx 30\%$, plotted for the last simulation snapshot: (A) carbon-carbon order parameter, (B) tail height in the z-direction, (C) area per lipid, and (D) curvature experienced by each lipid. Each bead corresponds to (A,B) the center of mass of an individual lipid tail or (C,D) the average center of mass of both tails.